ELSEVIER

Surface Science 368 (1996) 9–19

surface science

Vibrational dynamics of low frequency ($< 100\ cm^{-1}$) adsorbate motions

J.P. Culver [a,*], M. Li [b], R.M. Hochstrasser [b], A.G. Yodh [a]

[a] *Department of Physics, University of Pennsylvania, Philadelphia, PA 19104, USA*

[b] *Department of Chemistry and the Laboratory for Research on the Structure of Matter, University of Pennsylvania, Philadelphia, PA 19104, USA*

Received 1 May 1996; accepted for publication 1 August 1996

Abstract

Ultrafast time-resolved studies of the vibrational motions of CO on Cu(111) are described. In particular, the energy transfer rates between substrate electrons and phonons and the frustrated translation of CO are measured. An explicit relaxation model including the temperature dependence of these rates is developed and used in the analysis.

Keywords: Carbon monoxide; Copper; Vibrations of adsorbed molecules

1. Introduction

Generally, adsorbate vibrations couple to both the electronic and phonon degrees of freedom of a metal substrate. Theoretical and experimental studies have provided convincing evidence that a dynamical charge transfer mechanism is responsible for the coupling of adsorbate vibrations to substrate electron–hole pairs [1–3]. On the other hand, anharmonic couplings to phonons account for energy transfer between adsorbate and substrate vibrations [4–6]. We will discuss theory and measurement methodologies relevant to studies of energy transfer within the metal substrate/adsorbate complex. Inter-mode anharmonic couplings in particular will be considered as a means to assess the dynamics of low-frequency adsorbate modes.

We have conducted time-resolved infrared (IR) spectroscopic studies of $(\sqrt{3} \times \sqrt{3})$R30° CO molecularly adsorbed on Cu(111) just following visible excitation pulses of differing fluences. Observations of the CO vibrational response were obtained in situ on a state-specific basis, employing visible laser pulse excitations near the femtosecond desorption threshold. The transient vibrational dynamics of the low-frequency frustrated lateral-translation mode were monitored indirectly through its anharmonic effects on the higher-frequency CO stretch mode; in particular, the low-frequency mode is observed to induce calculable shifts in the complex frequency of the stretch modes as its amplitude is increased. This technique has been used to study the dynamics of the frustrated translation for CO on Cu(111) [7], Cu(100) [8] and Pt(111) [9] metal surfaces.

A new analysis is incorporated in this paper to interpret these observations. The model explicitly

* Corresponding author.

Published by Elsevier Science B.V.
PII S0039-6028(96)01023-0

employs the temperature-dependent coupling rate derived from a dynamical charge transfer model for electron–hole pair coupling to adsorbate vibrations. In principle, the couplings between adsorbate vibrations and substrate phonons are also temperature-dependent [5]. In the present experiments, however, the changes in the phonon temperature are small $\partial T_l/T_l \approx 0.1$, and the coupling rate γ_l between the frustrated translation and the Cu phonons is taken to be temperature-independent. Before discussing the experimental results we will review three theoretical topics; (i) e–h pair coupling to adsorbate vibrations, (ii) spectral signatures in the CO stretch mode due to thermal excitation of lower-frequency CO modes, and (iii) the response of the C–O stretch mode with a time-variant complex frequency to femtosecond IR probes.

2. Adsorbate vibrations coupling to metal substrate electron–hole pairs

The basic description of electron–hole pair interaction with adsorbate vibrations was introduced by Persson and Persson [1]. It involves the flow of charge between the substrate and a partially filled adsorbate electronic state (Fig. 1). Specifically for CO on Cu(111), the partially filled orbital is the $2\pi^*$ state. This state has been observed experimentally using inverse photoemission [10] and two-photon photoemission [11]. It lies ~ 3.35 eV above the Fermi level and has a width of $0.1\ \text{eV} < \Delta E < 0.6\ \text{eV}$.

Motion along each vibrational coordinate of the CO alters the occupancy of the $2\pi^*$ state since the electronic state mixing depends upon the particular positions of the adsorbate nuclei. Since the electronic and vibrational degrees of freedom are not completely separable, the dynamical charge transfer causes an exchange of energy between the adsorbate vibrations and the substrate electrons.

The relevant energy scales for this process are: (i) the energy of the partially filled adsorbate orbital (ε_a) relative to the metal Fermi level, (ii) the energy of the vibration ($\hbar\Omega$), and (iii) the thermal energy of the electrons (kT_e). Traditionally the dynamical charge transfer process has been considered in the regime where $kT_e \ll \hbar\Omega \ll \varepsilon_a$, and has been treated as a temperature-independent process [1,2]. Experimental studies have examined the energy relaxation of the high-frequency stretch vibrational mode for CO adsorbed on metal surfaces [3,12]. For the CO stretch mode, a zero-temperature model is appropriate in most situations of practical interest since $\hbar\Omega_{\text{stretch}}$ (~ 3000 K) is an order of magnitude larger than kT at room temperature. There are, however, situations in which the thermal energies in the adsorbate/substrate system become comparable with $\hbar\Omega$ and ε_a. For example, the low-frequency vibrational modes that arise when CO adsorbs on metal surfaces have energies of 30–400 cm^{-1}. The coupling of these vibrations to electron–hole pairs should be quite sensitive to the thermal distributions of the substrate electrons. In addition, intense femtosecond-visible pulses can generate transient thermal electrons with temperatures of up to ~ 5000 K. These temperatures are comparable to, or higher than, most vibrational energy levels and are within

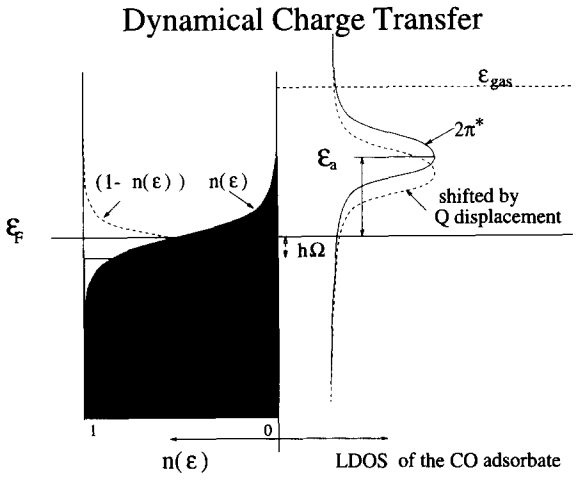

Fig. 1. The dynamical charge-transfer process is illustrated by the electronic density of states for the CO/Cu(111) system. Mixing with the substrate electrons causes the $2\pi^*$ level to lower and broaden in energy from the gas-phase value. Since the amount of hybridization depends on the positions of the adsorbate nuclei, movement along a vibrational coordinate Q will change the $2\pi^*$ local density of states (LDOS) and cause charge to flow between the CO and Cu(111) substrate. The relevant energies for this process are the energy of the vibration $\hbar\Omega$, the thermal spread of the Fermi function (kT_e), and the energy ε_a of the $2\pi^*$ LDOS.

an order of magnitude of ε_a for many adsorbates. Under these circumstances, thermal electrons making near resonant transitions can greatly enhance the energy-transfer process [13].

An expression for the coupling rate between an adsorbate vibration and the substrate electrons (γ_e) can be derived using the Andersson–Newns Hamiltonian description for the adsorbate hybridization and Fermi's golden rule [1,14]. Here we will focus on coupling to the frustrated translation (FT) vibration with mass-weighted coordinate Q (e.g. $Q^2 = \mu x^2$). The energy-transfer process involves a transition from vibrational state $n=1$ to $n=0$ and the scattering of an electron from an occupied hybrid adsorbate/substrate electronic state $|\alpha\rangle$ to an unoccupied hybrid state $|\beta\rangle$. Energy conservation requires that the difference in energy between the initial and final electronic states is equal to the vibrational energy of mode Q (e.g. $\varepsilon_\beta - \varepsilon_\alpha = \hbar\Omega$). The zero-temperature development of Persson [1] can be extended to non-zero temperatures by accounting for the occupied and unoccupied density of electronic states with the Fermi–Dirac distribution $n(\varepsilon) = 1/(1 + e^{(\varepsilon - \varepsilon_F)/kT})$. The mixed $|\alpha\rangle$ states are assumed to be populated as if they are bulk metal electronic states. Fermi's golden rule yields the following expression for the coupling rate

$$\gamma_e = \frac{2\pi}{\hbar} \sum_{\alpha\beta} \left| \langle \alpha, n=1 | H' | \beta, n=0 \rangle \right|^2 n(\varepsilon_\alpha)(1 - n(\varepsilon_\beta)) \times \delta(\varepsilon_\beta - \varepsilon_\alpha - \hbar\Omega). \quad (1)$$

Here, H' is the coupling term, and the wave functions $|\alpha,n\rangle$ represent the product of a hybrid state $|\alpha\rangle$, and a Q-mode vibrational state $|n\rangle$ [1]. The coupling rate can be rewritten in terms of the local density of states (LDOS) of the $2\pi^*$ orbital $\rho_a(\varepsilon)$

$$\gamma_e = \frac{2\pi}{\hbar} |\Delta_{aa}|^2 \int_{-\infty}^{\infty} d\varepsilon \rho_a(\varepsilon)\rho_a(\varepsilon + \hbar\Omega) n(\varepsilon) \times (1 - n(\varepsilon + \hbar\Omega)), \quad (2)$$

where

$$\Delta_{aa} = \frac{\partial \varepsilon_a'}{\partial Q} \sqrt{\frac{2\hbar}{\Omega}} = \frac{\partial \varepsilon_a'}{\partial Q} Q_0,$$

with Q_0 being the average zero-temperature displacement.

A temperature dependence is thus introduced through the temperature dependence of the Fermi distribution. This effect can be considered in two regimes, as depicted in Fig. 2. For temperatures much less than the energy of the $2\pi^*$ level ε_a, the LDOS ($\rho_a(\varepsilon)$) is essentially constant over the interval of integration in Eq. (2) [1,2]. The coupling rate is then expressed in terms of γ_e^0 and a temperature factor, i.e.

$$\gamma(T_e) = \frac{\gamma_e^0}{1 - e^{-\hbar\Omega/kT_e}}. \quad (3)$$

For temperatures approaching $\varepsilon_a/10$ or greater, the shape of the $2\pi^*$ LDOS must also be included. We model the LDOS as a Lorentzian with line center 3.35 eV above ε_F, and line width $\sim$0.6 eV [11]. Eq. (2) was integrated numerically and is depicted in Fig. 2. A sharp increase in the coupling strength occurs as the substrate electrons achieve thermal energies sufficient to make near-resonant transitions into the $2\pi^*$ band. For temperatures higher than ε_a, the resonant effect saturates and the coupling becomes less sensitive to temperature again. Similar resonance-enhanced couplings have been predicted by Brandbyge et al. [13] using a path integral technique to evaluate an electronic friction within a Langevin formalism. The resulting electron-temperature dependent adsorbate/substrate coupling was used to explain femtosecond laser desorption experimentals.

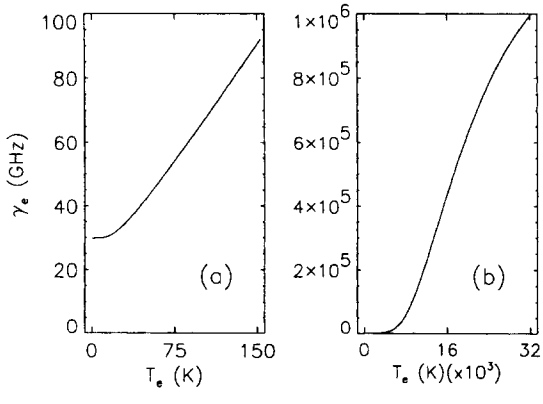

Fig. 2. Temperature dependence of γ_e predicted by the dynamical charge transfer model: (a) for $T_e \ll \varepsilon_a$, and (b) for $T_e \approx \varepsilon_a$.

3. Time-dependent dephasing of adsorbate vibrations

Though femtosecond probes have not yet been used for direct measurements of low-frequency motions, the low-frequency modes can be monitored indirectly. In this case the excitation of a low-frequency mode modifies the vibrational dynamics of some higher-frequency mode which may in turn be accessible to current ultrafast IR probes. This section discusses time-dependent dephasing of high-frequency modes due to anharmonic coupling to lower-frequency modes. When properly incorporated, this type of observation enables us to measure the coupling rates discussed in Section 2 between low-frequency adsorbate vibrations and the substrate electron and phonon reservoirs.

The temperature dependence of vibrational bands in polyatomic molecules is generally understood to arise from anharmonic coupling [15]. The molecular nuclear motions are coupled to each other and also to the bath modes. This situation permits any particular vibrational frequency to be modulated by the bath fluctuations, and hence yield line-shifting and line-broadening phenomena. In order to shift a high-frequency transition, a low-frequency mode with significant occupation number if required. The magnitude of the temperature shift or broadening will then depend on the size of the anharmonic coupling between the high- and low-frequency modes and the amplitude (i.e. occupation) of the low-frequency mode. The general theory that describes these circumstances is termed "exchange theory" [15,16]. In the present context the dynamics are regarded in terms of Brownian oscillator models [16,17].

For terminally bound CO on low-index metal surfaces, the CO stretch mode is predominantly dephased by the lateral frustrated translation (FT) of the CO complex. Recent density functional calculations indicate that the stretch mode has similar anharmonic couplings to both the frustrated rotation (FR) and the FT. However, since the frequency of the FT is about an order of magnitude smaller than the FR frequency, the thermal population and hence dephasing is an order of magnitude larger. For the specific case of the CO stretch coupling to the frustrated translation, the anharmonic coupling causes the FT frequency (Ω) to be lower when the CO stretch is excited than if it is not. Reciprocally, the actual CO stretch detuning frequency is $\Delta_{01}(Q) = \omega_{01}(Q) + \omega_L$, and is given by

$$\Delta_{01}(Q) = \Delta_{01} + (\zeta/\hbar)Q^2, \tag{4}$$

where $\zeta = \frac{1}{2}(\Omega_0^2 - \Omega_1^2)$ is a measure of the anharmonic coupling; Ω_v is the Brownian oscillator frequency in state v of the CO stretch, and Q is the FT normal-mode displacement. In considering the relaxation of the CO stretch, we treat the FT as a stochastically modulated displacement Q, that is considered to be a Brownian oscillator satisfying a Langevin equation. Because of the existence of anharmonic coupling between the CO stretch and the FT mode, the CO stretch frequency and thus the stretch density matrix elements ρ_{01} will be modulated. This is readily seen by considering the potential wells for the low-frequency Q-coordinate motion (Fig. 4). At higher temperatures the distribution of positions for FT is wider, which yields a smaller average frequency and broader linewidth for the stretch mode.

The polarization of the CO stretch layer can be obtained by considering the density matrix elements $\rho_{01}(t)$. For a layer of CO oscillators with dipole–dipole coupling and a stochastically modulated frequency, the following solution [7,16,18] for the ensemble average $\rho_{01} = \langle \sigma_{01} \rangle$ is obtained

$$\dot{\rho}_{01} = -\{i[\Delta_{01} + \delta(t)] + \gamma_0 + \gamma(t)\}\rho_{01}, \tag{5}$$

where $\delta(t)$ and $\gamma(t)$ can be written in terms of the average occupation number of the frustrated translation (n_{ft}).

$$\delta(t) = \delta\omega[n_{ft}(t)], \tag{6}$$

$$\gamma(t) = \frac{\delta\omega^2}{W}[n_{ft}(t)(n_{ft}(t)+1)]. \tag{7}$$

Here $\delta\omega = (\zeta/\hbar)Q_0^2$ and W is a term involving the dispersion of the CO stretch and the Brownian-oscillator relaxation time [18]. Since in this case the Brownian oscillator is coupled to two thermal baths, the time-dependent population of the frustrated translation mode n_{ft} is predicted using the following rate equation for a harmonic

oscillator

$$\dot{n}_{ft} = \gamma_e(n_e - n_{ft}) + \gamma_l(n_l - n_{ft}). \quad (8)$$

n_e and n_l represent the occupation numbers of the reservoir excitations at energy $\hbar\Omega$ for the instantaneous temperatures T_e and T_l, respectively [7]. γ_e and γ_l are the coupling rates of the frustrated translation to the substrate electrons and the phonon reservoirs, respectively. Previous experimental studies [7,8] have used a rate equation (Eq. (8)) with temperature-independent values of γ_e and γ_l. In contrast, this analysis utilizes a functional form derived earlier for γ_e which depends on the instantaneous value of substrate electron reservoir temperature T_e.

Eqs. (5)–(8) provide the propagator for the density matrix, from which the response to an IR probe field can be calculated. This will be discussed in Section 4. The only inputs needed are the time-variant substrate electron and lattice temperatures, T_e and T_l. These temperatures are calculated using a two-temperature model which has been discussed elsewhere. Examples of the T_e and T_l profiles obtained with typical laser pulses are shown in Fig. 3.

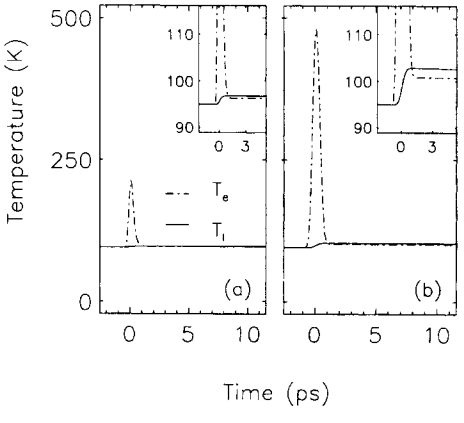

Fig. 3. The substrate temperatures, T_e and T_l, for our lowest (a) and highest (b) fluences. The energy initially deposited in the electrons creates a sharp peak in T_e. In contrast, the phonons have a much larger heat capacity and therefore experience a smaller temperature rise. Since T_e is modulated much more than T_l, T_e is more sensitive to changes in fluence. The measurements therefore probe the T_e-dependence of the coupling rate between the frustrated translation and the substrate electrons.

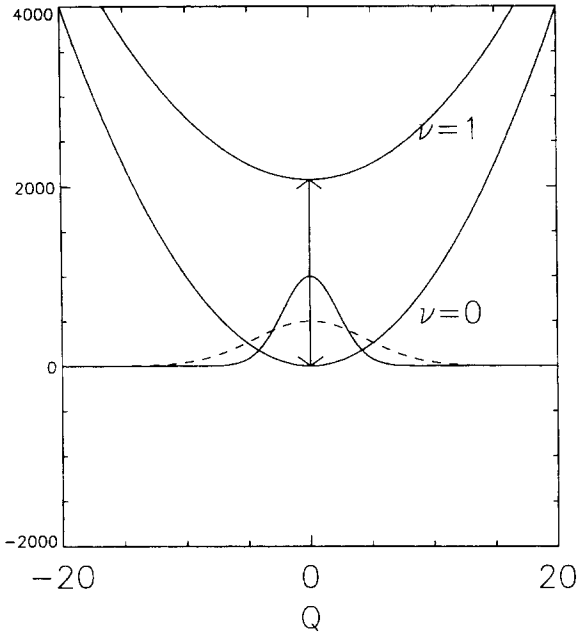

Fig. 4. Anharmonic coupling between the CO stretch and a low-frequency oscillator Q_i will modulate the frequencies of both modes. The frequency Ω_i of the coordinate Q_i oscillator is determined by the width of the potential wells. The frequency $\omega(Q_i)$ of the CO stretch mode is determined by the separation of the two potential surfaces. As $\langle Q^2 \rangle$ increases, the average stretch frequency decreases. Using a stochastic Brownian-oscillator model, the temperature dependence of the frequency shift can be obtained explicitly (see text).

4. Time-resolved IR probes

Ultrafast laser pulses which are shorter than the vibrational dephasing times of condensed phase systems are quite common. For example, spectral linewidths of vibrational transitions in the steady state are usually narrower than $\sim 20\ cm^{-1}$, corresponding to dephasing times longer than 500 fs. If vibrational states are caused to undergo changes on timescales less than 500 fs, it is evident that the interplay between the vibrational dephasing and the dynamical processes of interest must be considered as part of the interpretation of the experiment. In the particular case of CO on Cu(111) the free induction decay time, as measured by sum frequency generation, [19] is $T_2 = 2.2$ ps. This section addresses some issues related to the probing of perturbed vibrational transitions using ultrashort pulses. There are a variety of possible

approaches to obtaining transient IR spectra, and the experimental manifestations of the vibrational dephasing are dependent on the method used. Two approaches used in the study of IR transients are the short IR probe pulse method (see, for example, Refs. [8,12]), and the gated quasi-CW method (see, for example, Refs. [7,20,21]), which uses ultrafast gated IR detection. These approaches generally yield different signals from the same sample, so that a comparison of the advantages and disadvantages of each of them is worthwhile.

4.1. Modulation of the complex frequency in a two-level system

The simplest approach to calculating time-dependent vibrational spectra is to solve the damped Liouville equations (Bloch equations) for a two-level system with Hamiltonian

$$\mathscr{H} = \mathscr{H}_0 + S(t) + V(t), \tag{9}$$

where $\mathscr{H}_0$ is a two-level system with Bohr frequency $\omega_{10} = \omega_1 - \omega_0$, which in the present case will be a vibrational frequency. $S(t)$ is a time-dependent perturbation such as a first-order Stark effect which will usually be slow-acting compared with $V(t)$, the interaction of the two-level system with an electromagnetic field $E(t)$: i.e. $V(t) = -\mu_{01}E(t)$, where the field magnitude is $E(t) = \mathscr{E}(t)\cos(\omega t)$. For the experiments at hand, the frequency shifts will be due to modulations in a coupled low-frequency oscillator, as described in Section 3.

The Liouville equation for the off-diagonal elements of the density matrix in the representation of $\mathscr{H}_0$ or $\mathscr{H}_0 + S(t)$ is written with a time-dependent dephasing rate $\Gamma(t)$ as follows

$$\dot{\rho}_{01} = \frac{i}{\hbar}[\rho, \mathscr{H}]_{01} - \Gamma(t)\rho_{01} \tag{10}$$

$$= -\frac{i}{\hbar}(\rho_{00} - \rho_{11})\mu_{01}E(t) - (i\omega_{01}(t) + \Gamma(t))\rho_{01}. \tag{11}$$

For weak probe fields, the population will stay in the ground state and we can assume that $n_0 = \rho_{00} - \rho_{11}$ remains constant. Integration of Eq. (11) yields:

$$e^{-i\omega_L t}\rho_{01}(t) = \frac{i\mu_{01}n_0}{\hbar}\int_{-\infty}^{t} dt_1 E(t_1)\, e^{-\int_{t_1}^{t} d\tau (i\omega_{01}(\tau) + \Gamma(\tau))}, \tag{12}$$

where $\omega_{01}(\tau) = \omega_{01} + \frac{1}{\hbar}[S_{00}(\tau) - S_{11}(\tau)]$

represents the frequency modulated by the time-dependent Stark shift.

The two experimental approaches considered are the gated quasi-CW probe pulse and the short probe pulse filtered by a monochromator. These two methods can be explored by taking the short and long pulse limits of a Gaussian pulse expression for the probe IR pulse. A Gaussian probe pulse with shape $E(t) = \mathscr{E}_0\, e^{-a(t-t_{pr})^2 + i\omega_1(t-t_{pr})}$ and pulse duration $\tau_p = \sqrt{(2\ln 2)/a}$ substituted into Eq. (12) will generate the following polarization

$$e^{-i\omega_1(t-t_{pr})}\rho_{01}(t) = \frac{i\mu_{01}n_0\mathscr{E}_0}{\hbar} \times \int_{-\infty}^{t} dt_1 e^{-a(t-t_{pr})^2}\, e^{-\int_{t_1}^{t} d\tau \Omega_{01}(\tau)},$$

where $\Omega_{01}(\tau) = i(\omega_{01}(\tau) + \omega_L) + \Gamma(\tau)$. (13)

We now compare the two different experimental approaches to measuring $\rho_{01}(t)$ or its spectra. The inclusion of substrate effects has been considered elsewhere [7], and for simplicity we consider here a sample probed in transmission. When short probe pulses are employed in the experiment, the envelope $\mathscr{E}(t)$ is finite and presumably has a duration shorter than the dynamics of interest. On the other hand, with the gating technique, the IR field is quasi-monochromatic and $\mathscr{E}(t) = \mathscr{E}_0$ is effectively a constant over the time scale of the experiment. As can be seen from the exponentials inside the integral, the detuning ($\Delta_{01} = \omega_{01} + \omega_1$) and the decay time $\gamma(\tau)$ are the physical constants which define the relevant time scales. While typical experimental values of the pulse duration and $|\Omega_{01}|$ may not provide for completely separated time-scales, to illustrate the basic nature of the two

approaches, the limits $\sqrt{a} \gg |\Omega_{01}|$ and $\sqrt{a} \ll |\Omega_{01}|$ are taken.

4.1.1. Gated quasi-CW probe

For the gated quasi-CW probe the long pulse limit, $\sqrt{a} \ll |\Omega_{01}|$, is taken. In this limit the polarization of the adsorbate can be written

$$e^{-i\omega_1(t-t_{pr})}\rho_{01}(t) = \frac{i\mu_{01}n_0\mathscr{E}_0}{\hbar}\int_{-\infty}^{t} dt_1\, e^{-\int_{t_1}^{t} d\tau \Omega_{01}(\tau)}. \tag{14}$$

The resulting quasi-CW infrared beam is gated by up- or down-conversion in a non-linear crystal after the sample by mixing with a short visible pulse having field envelope $\mathscr{E}(t-t_g)$ centered at the gating or delay time t_g. If the gating pulse is very short compared with the relevant dynamics, and if the signal is small, then the detected light intensity is given approximately by

$$I(t_g) \propto \mathscr{E}_0^2 + 2\mathscr{E}_0\mathscr{E}_{gen}(t_g). \tag{15}$$

The in-phase part of the generated field envelope is proportional to $\mathrm{Im}\{\rho_{01}\, e^{-i\omega_L(t_g-t_{pr})}\}$, which is obtainable directly from Eq. (14) with $t = t_g$. For the CW method, the field is, apart from constants

$$\mathscr{E}_{gen}(t_g) = \mathrm{Im}\left\{ i\int_{-\infty}^{t_g} dt_1\, e^{-\int_{t_1}^{t_g} d\Omega_{01}(\tau)d\tau} \right\}. \tag{16}$$

In general we are interested in the differential change in absorption due to a pump pulse, so the signal is

$$\mathrm{Signal}(t) = \frac{I_{pumped}}{I_0} - \frac{I_{unpumped}}{I_0} \tag{17}$$

$$\approx \mathrm{Re}\left\{ \int_{-\infty}^{t_g} dt_1\, e^{-\int_{t_1}^{t_g} d\Omega_{01}(\tau)d\tau} - \frac{1}{\Omega_{01}^0} \right\}, \tag{18}$$

where Ω_{01}^0 is for the unpumped case.

4.1.2. Short pulse probe

The situation for a short pulse probe signal is qualitatively different from Eq. (16). Assuming that the pulse is Gaussian and much shorter than the modulations in the IR response ($\sqrt{a} \gg |\Omega_{01}|$), we can write the generated field for time $t > t_{pr}$

$$E_{gen}(t, t_{pr}) \approx \mathscr{E}_0\sqrt{\frac{\pi}{a}}\, e^{-\int_{t_{pr}}^{t} d\tau (i\omega_{01}(\tau)+\gamma(\tau))}. \tag{19}$$

The spectrum of the generated field is given by its Fourier transform. This can be expressed using a complex frequency, $\Omega_{01}^F(t) = i(\omega_{01}(t) + \omega_F + \Gamma(t)$, such that

$$\mathscr{E}_{gen}(\omega_F, t_{pr}) = \mathscr{E}_0\sqrt{\frac{\pi}{a}}\int_{t_{pr}}^{\infty} dt_1\, e^{-\int_{t_{pr}}^{t_1} d\tau(\Omega_{01}^F(\tau))}. \tag{20}$$

Again using unpumped measurements as a reference, the signal obtained is

$$\mathrm{Signal}(t) \approx \mathrm{Re}\left\{ \int_{t_{pr}}^{\infty} dt_1\, e^{-\int_{t_{pr}}^{t_1} d\tau(\Omega_{01}^F(\tau))} - \frac{1}{\Omega_{01}^F} \right\}. \tag{21}$$

4.2. Model of an impulsive complex frequency shift

The signals described in Section 4.1.2 can be easily calculated numerically for arbitrary pulses and functions $S(t)$ and $\Gamma(t)$. However, to illustrate the nature of the transient coherent effects involved, we now compare the two experiments using δ-function pump pulses that produce step-function changes in Ω_{01}.

With the conditions of δ-function pump and gating pulses, separated by $\tau_d = t_g - t_{pump}$, the differential reflectivity signal in the gated quasi-CW experiment is readily obtained from Eq. (18)

$$\tau_d < 0; \qquad S = 0, \tag{22}$$

$$\tau_d > 0; \qquad S = \mathrm{Re}\left\{ \left(\frac{1}{\Omega_b} - \frac{1}{\Omega_a} \right)[1 - e^{-\Omega_b\tau_d}] \right\}, \tag{23}$$

where $\Omega_a = i\Delta_{01}^a + \gamma_a$ and $\Omega_b = i\Delta_{01}^b + \gamma_b$ are the

complex frequencies before and after the pump pulse. Eq. (23) determines how quickly the new signal can be observed and how suddenly the original absorbance, characterized by Ω_a, can disappear as a result of change in the complex frequency. Notice that the dynamics are determined by the *new* complex frequency. Simulations for three different frequency shifts are shown in Fig. 5.

The short probe pulse method (Eq. (21)) with time delay $\tau_d = t_{pr} - t_{pump}$, and the selection of a frequency initially detuned by complex frequency Ω_a^F from resonance, yields the signal intensity as follows

$$\tau_d < 0; \qquad S = \mathrm{Re}\left\{\left(\frac{1}{\Omega_b^F} - \frac{1}{\Omega_a^F}\right) e^{\Omega_a^F \tau_d}\right\}, \tag{24}$$

$$\tau_d > 0; \qquad S = \mathrm{Re}\left\{\left(\frac{1}{\Omega_b^F} - \frac{1}{\Omega_a^F}\right)\right\}. \tag{25}$$

The $\tau_d < 0$ term of Eq. (24), and hence the time-dependence of these signals, always grows in with time constant determined by the unperturbed resonance frequency Ω_a^F, and the peak signal occurs at zero delay of pump and probe pulses. Simulations for three different frequency shifts are shown in Fig. 5.

Consider some qualitative features of the two approaches. The short pulse probe signal evolution is always shaped initially by the unpumped vibrational properties in Ω_a^F. In contrast, the time dependence of the quasi-CW signal is determined by Ω_b. Fig. 5a shows the signals expected for the case where the absorption width is suddenly increased. The only effect this increase has on the short pulse probe signal is on its amplitude at zero delay. On the other hand, the gated GW method yields a signal growth kinetics that depends on the amount of line broadening that occurred. In the second example the perturbation causes an instantaneous line shift which is small compared to the linewidth, and the linewidth remains constant (Fig. 5b). Again the short pulse probe signal (bleach) grows up to zero delay in accordance with $e^{\gamma_a \tau_d}$ and is constant thereafter at a level determined by the magnitude of the frequency shift. The gated-CW method provides a similar signal, but it grows after time zero. Both signals grow in

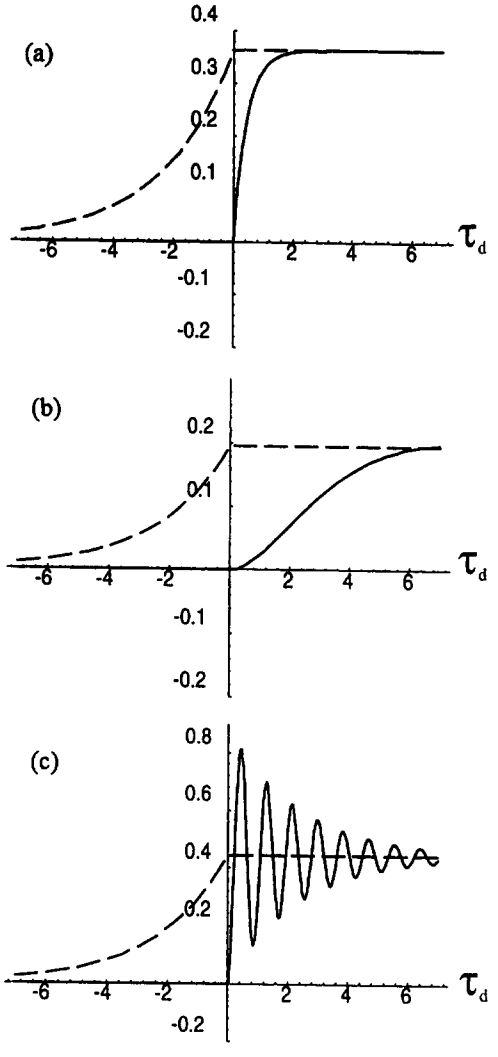

Fig. 5. Simulations of an impulsive frequency response for three different complex frequency shifts. For the gated CW method (dashed line) the laser frequency is at 2075 cm^{-1}. For the short probe pulse method, the filter frequency is at 2075 cm^{-1}. (a) Increase in line width, $\gamma_a = 2.25\ cm^{-1}$, $\gamma_b = 12.25\ cm^{-1}$, and $\omega_{01}^a = \omega_{01}^b = 2074$. (b) Center frequency shift of ~50% the linewidth $\gamma_a = \gamma_b = 2.25\ cm^{-1}$, $\omega_{01}^a = 2074\ cm^{-1}$, and $\omega_{01}^b = 2072\ cm^{-1}$. (c) Center frequency shift of ~5× the linewidth, $\gamma_a = \gamma_b = 2.25\ cm^{-1}$, $\omega_{01}^a = 2074\ cm^{-1}$, and $\omega_{01}^b = 2001\ cm^{-1}$.

with the same response time. In this case the information about the line shifting comes purely from the magnitude of the signal, and can be similarly obtained from either approach. The responses to a large frequency shift are shown in

Fig. 5c. The short-pulse measurement shows similar dynamics to the small frequency shift with a different signal magnitude. A quite different response is expected from the quasi-CW method, which will exhibit damped oscillations with period corresponding to the detuning frequency. If this shift is sufficiently large that the time resolution is insufficient to isolate the beats, or if the sample is sufficiently inhomogeneous, then an instantaneous change in absorbance will be sensed. An example of this effect was observed in the experiment on the photodissociation of carbon monoxide from an iron carbonyl [22]. On dissociation, the resonance frequency shifts in about 50 fs from 1951 to 2135 cm^{-1} without much change in width. This shift of 184 cm^{-1} corresponds to a beat period of 180 fs which could not have been resolved in that experiment, so an "instantaneous" bleach signal is observed. These appear in much the same way as the population changes would (see Ref. [7]). This is an example where the population kinetics give a reasonable interpretation of spectral changes. In contrast, the short-pulse probe method monitoring dissociation will yield a coherence artifact at negative time similar to that shown in Fig. 5c. Thus it is better to monitor the disappearance of molecules using the gated quasi-CW probe.

5. Description of measurement

Our experimental technique has been described in detail elsewhere [7], and is therefore only briefly outlined here. The experiment involves heating the substrate with a short visible light pulse and monitoring the adsorbate response using time-resolved infrared spectroscopy. Measurements were taken at various levels of substrate excitation. The visible pulse fluence was ultimately increased to a level which induced the desorption of CO.

For Cu substrates, the nascent distribution of electrons excited by direct interaction with the visible pulse thermalizes in $\lesssim 70$ fs [23,24]. On longer timescales, relevant to the present experiments, the metal response is described by a model with separate electron (T_e) and phonon (T_l) temperatures [25,26]. These substrate reservoirs have markedly different temporal profiles, which are indicated in Fig. 3 for a typical excitation pulse [27].

The CO overlayer is probed by a quasi-CW infrared pulse (30 ps) tuned near the CO stretch frequency. The reflected IR field intensity records the adsorbate susceptibility and is time-resolved by up-conversion in a nonlinear crystal using a 500 fs visible gating pulse.

Data were taken at several frequencies for each fluence in order to increase the accuracy of the numbers reported. Some examples of the data obtained with a pump pulse fluence absorbed of $F_{abs} = 0.18$ mJ cm^{-2} are shown in Fig. 6. The basic spectral feature is brought about by a shifting Lorentzian absorption profile which exhibits a maximum shift at around 2 ps, and returns to an offset value within the next 10 ps. At fluences higher than $F_{abs} = 0.33$ mJ cm^{-2}, the total signal level decreased over successive time scans (~ 10 min), indicating desorption of the CO. For the fluences in the range 0.054–0.33 mJ cm^{-2} the data clearly agree with the qualitative aspects of the time-dependent exchange picture [7].

To use the temperature-dependent coupling rate of Eq. (3), it is necessary to know the value of $\hbar\Omega$. Our FTIR measurements interpreted in the context of an exchange model [15,17] establish an upper limit of $\hbar\Omega < 60$ cm^{-1} [7]. Additional insight into the value of $\hbar\Omega$ is obtained by considering the experimentally determined values of the frustrated translation for atop CO on Cu(100) [8], Pt(111) [28] and Ni(111) [28]. For all of these systems the frequency lies between 30 and 60 cm^{-1}, and fits were carried out for $\hbar\Omega$ values within this range.

Instead of fitting with a temperature-independent rate, the data were fit for γ_e^0 of Eq. (3). An intermediate value of $\hbar\Omega = 45$ cm^{-1} was used to obtain the best fit value for the zero-temperature coupling rate of $\gamma_e^0 = 25 \pm 7$ GHz. The result was obtained using all possible light fluences. Coupling to the phonons was found to be $\gamma_l = 280 \pm 100$ GHz. The fluences were fitted and determined largely by the magnitude of the signal. The 95 K value for the coupling rate, $\gamma_e(95) = 50$ GHz, is lower than the value $\gamma_e = 145$ GHz, obtained using a temperature-independent analysis with the same physical constants [27]. Within the errors quoted, the same value of γ_e^0 was found for all fluences. Thus the

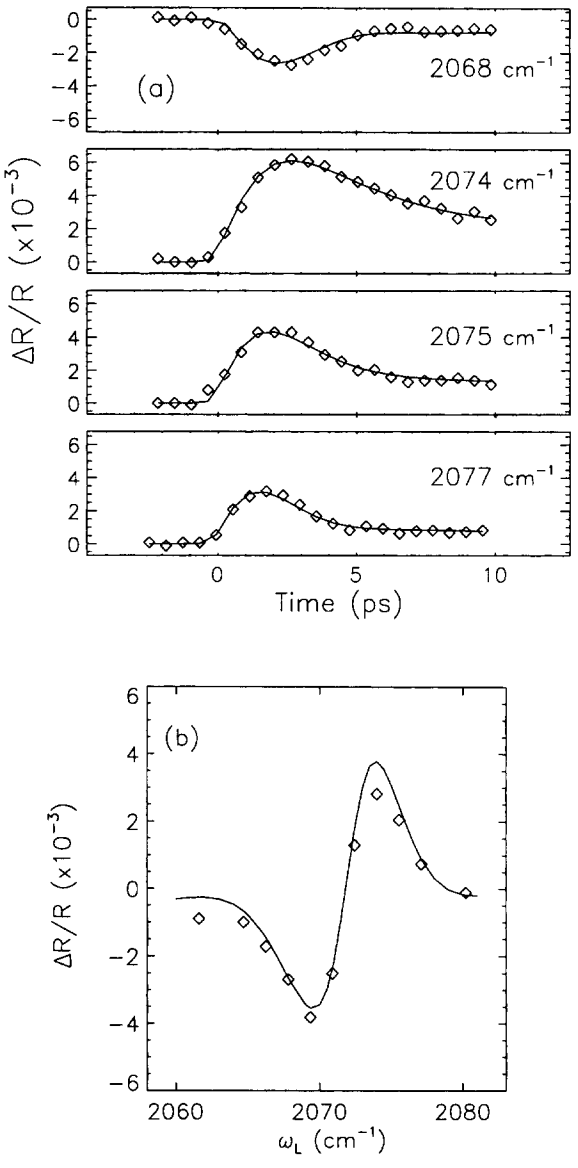

Fig. 6. Transient fractional difference reflectivity of CO on Cu(111). (a) Time scans as a function of probe laser frequency. (b) Frequency scan taken at fixed time delay of 3 ps.

excitation dependence of the CO response is well accounted for by the dynamical charge-transfer model. The error bars are derived from nonlinear least-squares fitting of the data. However, the value of γ_0^0 is subject to the uncertainty of two physical parameters encountered in the full fitting procedure. As has been discussed previously, the range of experimental values for the electron–phonon coupling constant affects the value of γ_e^0 [8]. In the present analysis an intermediate value of $G = 0.7\ \mathrm{W\,m^{-3}\,K^{-1}}$ has been used. For the values of G at the ends of the experimental range ($G = 0.3$–$1.0\ \mathrm{W\,m^{-3}\,K^{-1}}$), we find $\gamma_e^0 = 10(+6\ -2)$ GHz and, $\gamma_e^0 = 30 \pm 7$ GHz, respectively. The zero-temperature rate γ_e^0 also depends on $\hbar\Omega$, and for the values at the ends of the range $\hbar\Omega = 30$–$60\ \mathrm{cm^{-1}}$, we find $\gamma_e^0 = 21 \pm 7$ GHz and $\gamma_e^0 = 33 \pm 7$ GHz, respectively. As noted above, we are assuming the coupled mode is harmonic. No experimental information yet exists to test this assumption.

The most recent theoretical predictions for γ_e are molecular dynamics (MD) calculations which incorporate electronic friction. These calculations predict a $\gamma_e = 23$ GHz for $T = 10$ K and $\gamma_e = 43$ GHz for $T = 150$ K [5]. Allowing for the uncertainty in the electron–phonon coupling rate, these are in reasonable agreement with our findings. The most recent calculations for γ_1 are density functional (DF) calculations, which have a more complete treatment of the electrons than the MD calculations, and also use a slab geometry to better capture the periodic nature of the surface. The DF theory predicts a value of $\gamma_1 = 333$ GHz, which is in good agreement with our results.

6. Conclusion

In this paper we have discussed a novel way to measure the coupling rate of low-frequency ($< 100\ \mathrm{cm^{-1}}$) adsorbate vibrations to the substrate electrons and phonons. Low-frequency adsorbate-like modes are often of much interest, particularly because they are the modes which, when sufficiently excited, lead to desorption and diffusion. Recently, both helium atom scattering [29] and CW far-IR [30] experiments have examined the low-frequency vibrational dynamics of CO on Cu. However the CO stretch mode, with $\hbar\omega \approx 2000\ \mathrm{cm^{-1}}$, is the only CO complex vibration to be directly monitored by ultrafast IR spectroscopy thus far. The experimental method we have described exploits the frequency shift of the stretch vibration induced by the frustrated translation mode. By monitoring the temperature of the frustrated translation, via the stretch frequency shift, ultrafast measurements

of the relaxation of a sub-100 cm^{-1} vibration were obtained. As evidenced by these results, combining the novel environment created by femtosecond visible excitation of surfaces with the detailed mode-specific descriptions of IR spectroscopy, much can be learned about ultrafast surface photoprocesses.

Acknowledgements

It is a pleasure to acknowledge useful conversations with Paul Soven. This work has been supported by the NSF MRL program through Grant #DMR-9120668. A.G.Y. acknowledges partial support from the NSF through the PYI Program, and from the Alfred P. Sloan Foundation. R.M.H. acknowledges partial support through grants from the NIH and the NSF.

References

[1] B.N.J. Persson and M. Persson, Solid State Commun. 36 (1980) 175.
[2] M. Head-Gordon and J.C. Tully, J. Chem. Phys. 96 (1992) 3939.
[3] A.L. Harris, N.J. Levinos, L. Rothberg, L.H. Dubois, L. Dhar, S.F. Shane and M.J. Morin, J. Electron Spectrosc. 54/55 (1990) 5.
A.L. Harris, L. Rothberg, L. Dhar, N.J. Levinos and L.H. Dubois, J. Chem. Phys. 94 (1991) 2438.
M. Morin, N.J. Levinos and A.L. Harris, J. Chem. Phys. 96 (1992) 3950.
[4] P. Guyot-Sionnest, P. Dumas, Y.J. Chabal and G.S. Higashi, Phys. Rev. Lett. 64 (1990) 2156.
[5] J.C. Tully, M. Gomez and M. Head-Gordon, J. Vac. Sci. Technol. A 11 (1993) 1914.
[6] S.P. Lewis and A.M. Rappe, to be published.
[7] J.P. Culver, M. Li, L.G. Jahn, R.M. Hochstrasser and A.G. Yodh, Chem. Phys. Lett. 214 (1993) 431.
J.P. Culver, M. Li, L.G. Jahn, R.M. Hochstrasser and A.G. Yodh, in: Laser Spectroscopy and Photochemistry on Metal Surfaces, Eds. H.-L. Dai and W. Ho (World Scientific, Singapore, 1995) p. 542.
[8] T.A. Germer, J.C. Stephenson, E.J. Heilweil and R.R. Cavanagh, Phys. Rev. Lett. 71 (1993) 3327; J. Chem. Phys. 101 (1994) 1704.
[9] T.A. Germer, J.C. Stephenson, E.J. Heilweil and R.R. Cavanagh, J. Chem. Phys. 98 (1993) 9986.
[10] P. Avouris and R.E. Walkup, Annu. Rev. Phys. Chem. 40 (1989) 173.
[11] T. Hertel, E. Knoesel, E. Hasselbrink, M. Wolf and G. Ertl, Surf. Sci. 317 (1994) L1147.
E. Knoesel, T. Hertel, M. Wolf and G. Ertl, Chem. Phys. Lett. 240 (1995) 409.
[12] J.D. Beckerle, M.P. Casassa, R.R. Cavanaugh, E.J. Heilweil and J.C. Stephenson, Phys. Rev. Lett. 64 (1990) 2090.
J.D. Beckerle, M.P. Casassa, E.J. Heilweil, R.R. Cavanaugh and J.C. Stephenson, J. Electron Spectrosc. 54/55 (1990) 17.zl
[13] M. Brandbyge, P. Hedegard, T.F. Heinz, J.A. Misewich and D.M. Newns, to be published.
[14] J.P. Culver, M. Li, Z.-J. Sun, R.M. Hochstrasser and A.G. Yodh, Chem. Phys. 205 (1006) 159.
[15] C.B. Harris, R.M. Shelby and P.A. Cornelius, Phys. Rev. Lett. 38 (1977) 1415.
R.M. Shelby, C.B. Harris and P. Cornelius, J. Chem. Phys. 70 (1974) 34.
S. Marks, P.A. Cornelius and C.B. Harris, J. Chem. Phys. 73 (1980) 3069.
[16] N.G. van Kampen, Stochastic Processes in Physics and Chemistry (North-Holland, New York, 1981).
[17] B.N.J. Perrson and R. Ryberg, Phys. Rev. B. 32 (1985) 3586.
[18] B.N.J. Perrson, F.M. Hoffman and R. Ryberg, Phys. Rev. B. 34 (1986) 2266.
[19] J.C. Owrutsky, J.P. Culver, M. Li, Y.R. Kim, M.J. Sarisky, M.S. Yeganeh, A.G. Yodh and R.M. Hochstrasser, J. Chem. Phys. 97 (1992) 4421.
[20] J.N. Moore, P.A. Hansen and R.M. Hochstrasser, Chem. Phys. Lett. 138 (1987) 110.
[21] M. Li, J.C. Owrutsky, M. Sarisky, J.P. Culver, A. Yodh and R.M. Hochstrasser, J. Chem. Phys. 98 (1993) 5499.
[22] P.A. Anfinrud, C. Han and R.M. Hochstrasser, Proc. Natl. Acad. Sci. USA 86 (1989) 8387.
[23] W.W. Fann, R. Storz, H.W.K. Tom and J. Bokor, Phys. Rev. Lett. 68 (1992) 2834.
[24] C.A. Shmuttenmaer, M. Aeschlimann, H.E. Elsayed-Ali, R.J.D. Miller, D.A. Mantell, J. Cao and Y. Gao, Phys. Rev. B 50 (1995) 8957.
[25] S.I. Anisimov, B.L. Kapeliovich and T.L. Perel'man, Zh. Eksp. Teor. Fiz. 66 (1974) 776.
[26] H.E. Elsayed-Ali, T. Norris, M.A. Pessot and G. Mourou, Phys. Rev. Lett. 58 (1987) 1212.
[27] The following physical constants were used: electron phonon coupling $G = 0.7 \times 10^{17}$ W m^3 K^{-1}, phonon heat capacity $C_l = 2.26 \times 10^6$ J m^{-3} K^{-1}, electron heat capacity $C_e = 96.6 T_e$ J m^{-3} K^{-2}, electron diffusion constant $\kappa = 435 T_e/T_l$ W m^{-1} K^{-1}.
[28] A.M. Lahee, J.P. Toennies and C. Woll, Surf. Sci. 177 (1986) 371.
[29] A. Graham, F. Hoffman and J.P. Toennies, J. Phys. Chem. 104 (1996) 5311.
[30] C.J. Hirschmugl and G.P. Williams, Phys. Rev. B 52 (1995) 14177.